International Journal of Power Electronics and Drive System (IJPEDS)
Vol. 17, No. 4, December 2026, pp. 3034~3043
ISSN: 2088-8694, DOI: 10.11591/ijpeds.v17.i4.pp3034-3043

Robust bearing fault diagnosis under low sampling conditions via physics-informed feature engineering and optimized SVM with discriminant learning

Gigih Priyandoko[1], Aviv Yuniar Rahman[2]
[1]Department of Electrical Engineering, Faculty of Engineering, Universitas Widya Gama, Malang, Indonesia
[2]Department of Informatics Engineering, Faculty of Science and Technology Informatics, Universitas Widya Gama, Malang, Indonesia

Article Info

Article history:

Received Apr 17, 2026
Revised Aug 22, 2026
Accepted Sep 17, 2026

Keywords:

Bearing fault
LDA
Low sampling
MCSA
SVM

ABSTRACT

The evaluation of bearing condition through low-rate current assessments is appealing for economical motor oversight, though 10 Hz data collection is unable to identify the traditional high-frequency bearing elements employed in spectral MCSA. This research evaluates whether slower current envelope and statistical variations remain discriminative. The proposed pipeline combines several different features, including statistical, entropy, autoregressive, Teager energy operator, and ball-oriented descriptors. These are combined with Fisher-score feature selection, linear discriminant analysis, and an RBF support vector machine with confidence-weighted trial voting. Twenty-one independent laboratory trials were analyzed, including seven healthy trials, seven ball-fault trials, and seven inner-race-fault trials. The data were split into seven groups, with each group having one full trial in each group. All of the data preparation, feature selection, and model tuning were done in the training group. The configuration that was selected yielded 70/72 accurate out-of-fold window predictions (97.22%; Wilson 95% CI: 90.4-99.2%) and 21/21 correct trial decisions (100%; Wilson 95% CI: 84.5-100%). Trial-level accuracy was 100% in every outer fold (mean 100%, SD 0 percentage points); however, this reflects only three test trials per fold. The results show that this is possible in one controlled motor-bearing setup, but not in terms of external robustness or the direct recovery of the bearing's characteristic frequencies. Before industrial generalization, validation across motors, loads, noise levels, fault severities, and an external dataset is required.

This is an open access article under the CC BY-SA license.

Corresponding Author:

Gigih Priyandoko
Department of Electrical Engineering, Faculty of Engineering, Universitas Widya Gama
Malang, Indonesia
Email: gigih@widyagama.ac.id

1. INTRODUCTION

Robust and economical, induction motors are central to industrial drives, manufacturing systems, and energy-conversion equipment. However, unplanned downtime and maintenance costs are often caused by bearing degradation [1]-[6]. Vibration monitoring is susceptible to mechanical defects, whereas motor current signature analysis (MCSA) proffers a non-invasive alternative by utilising electrical measurements that are already extant in many drive systems [7]-[10]. The greatest practical challenge lies in low-cost installations, where sensing bandwidth, labelled fault data, and computational resources are limited [11], [12].

The current state of research in bearing diagnosis involves a variety of approaches, including the use of wavelet and wavelet-scattering representations [13], [14] statistical or autoregressive features with

classical classifiers [15], [16], physics-guided and attention-based neural network applications [17], [18], entropy-based hybrid learning [18]-[21], lightweight architectures [22]-[24], discriminative feature selection [25], [26], few-shot learning under noisy data [27], [28], and explicit studies of noise effects in electrical-machine diagnosis [29]. These approaches have been organised by signal, representation, classifier, strength, and limitation in Table 1.

The unsolved problem is whether information used for diagnosis is contained in a current record sampled at 10 Hz, when only 21 independent trials are available. A 10 Hz record has a 5 Hz Nyquist limit; therefore, the estimated bearing characteristic frequencies cannot be represented directly. The results of overlapping windows can be optimistic if the windows from one acquisition are split between the training and test sets. Therefore, the scientific question is not whether conventional spectral MCSA is reproduced by low-rate sensing, but whether leakage-controlled preliminary classification is supported by slower current modulation and statistical structure.

To solve this problem, the study proposes a system that integrates various types of information about the data. This system uses statistical, entropy, autoregressive, and ball-oriented descriptors, as well as a Teager energy operator (TEO) and Fisher-score feature selection. It also uses linear discriminant analysis and a radial basis function-support vector machine (RBF-SVM) with confidence-weighted trial voting. Unlike a CNN, which learns a latent representation from start to finish, the proposed descriptors are interpretable and can be inspected individually. Each data-dependent transformation is fitted within the training fold, setting this feature stack apart from a generic one. While this distinction demonstrates the novelty of the framework, it does not prove that it outperforms CNN, hybrid ensemble, or conventional MCSA methods without a common benchmark.

The objective of the research is the establishment of the capability of the suggested low-rate feature-engineering and grouped-classification framework to differentiate between healthy, ball-fault, and inner-race-fault trials under one controlled motor-bearing configuration, while stopping window-level leakage and reporting statistical uncertainty. The contributions are as follows:

- The 10 Hz data have been reinterpreted as low-frequency current-trend information.
- A Fisher-linear discriminant analysis (LDA)-(SVM) workflow has been developed for use with small datasets.
- A trial-grouped confidence-weighted aggregation method has been created, with fold-level and confidence-interval reporting.
- The expected outcome is not a claim of industrial generalizability, but rather feasibility evidence and a reproducible basis for multirate, noise-sensitivity, and external validation.

Table 1. Recent methods used to diagnose bearing faults (2021–2026)

No	Year	Method	Signal type	Feature type	Classifier	Strengths	Limitations
1	2021 [13]	Wavelet packet energy + SVM	Vibration	Time–frequency energy	SVM	High resolution in the frequency domain, effective for periodic faults	Requires a high sampling rate, not suitable for low-sampling MCSA
2	2022 [14]	Wavelet scattering transform + SVM	Current/ vibration	Scattering features	SVM	Robust to noise and signal deformation	Less sensitive to weak impulsive faults
3	2023 [15]	Random forest + statistical features	Current	Statistical features	RF	Robust, simple, low computational cost	Feature overlap for complex faults
4	2024 [16]	MCSA + SVM	Current	AR + statistical	SVM	Good for periodic faults (inner race)	Weak for Ball fault (non-periodic)
5	2025 [16]	Physics-Guided CNN	Multi-modal	Hybrid physics + deep features	CNN	Improved interpretability and accuracy	Not suitable for small datasets
6	2025 [18]	Entropy + ensemble learning	Current	Entropy-based	Ensemble	Better noise robustness	Still struggles with low SNR faults
7	2026 (Proposed)	Feature engineering + Fisher selection + LDA + optimized SVM + voting	Current (10 Hz)	Statistical + Entropy + AR + TEO + Ball-specific	SVM (RBF)	Promising accuracy in the present 10 Hz laboratory dataset	Only 21 controlled trials; no external or head-to-head validation

2. METHOD

2.1. Research design

The study's use of a controlled experimental and data-driven design is for the assessment of the remaining usability of weak bearing-fault information in three-phase motor-current signals sampled at 10 Hz. The unit of independence is the acquisition trial rather than an overlapping signal window. To ensure that windows derived from one acquisition cannot appear simultaneously in training and test data, model

development and validation are organized by trial identifiers. The workflow is designed to evaluate feature representation, class separation, and classification at both window and trial levels. It does this while retaining the practical constraints of low-cost sensing and a small dataset.

2.2. Data sources

The dataset comprises synchronized three-phase current records from a 1.5 HP, 220–230 V, 50 Hz, four-pole induction motor with a 6203Z bearing operating at approximately 1400 rpm. Three conditions were examined: healthy, ball fault, and inner-race fault. Seven independent acquisitions were recorded per condition, producing 21 trial-level experimental units. Each trial was assigned a unique group identifier before windowing. The acquisition interface was based on an Arduino Mega and stored one three-phase observation every 0.1 seconds (10 Hz). This rate is below that required to resolve the 50 Hz carrier frequency or the theoretical bearing characteristic frequencies. Consequently, the stored series must be interpreted as a low-rate current trend/envelope representation rather than a raw waveform maximum-component spectral analysis (MCSA). The feature matrix X, label vector Y, and trial-group vector G were constructed only after this scope restriction was defined.

Justification and limitations of the sampling rate. At 1400 rpm, the shaft frequency is approximately 23.33 Hz. With eight rolling elements, a ball diameter of 6 mm, a pitch diameter of 30 mm, and an assumed contact angle of almost 0°, the standard kinematic estimates are around 74.7 Hz for the outer race ball-pass frequency and 112.0 Hz for the inner race ball-pass frequency. Both of these values exceed the 5 Hz Nyquist limit of a 10 Hz recording. Therefore, the present method does not claim to directly observe these characteristic frequencies. Any discrimination must therefore arise from slower load-current modulation, envelope variation, stochastic energy, or condition-dependent statistical structure. It is important to note that this experiment tests low-rate condition classification, not conventional high-frequency spectral bearing diagnosis.

The choice of 10 Hz represents the bandwidth of the available low-cost acquisition system rather than the optimum sampling rate for bearing diagnosis. While it reduces storage and computation requirements, it also introduces serious information constraints and possible aliasing. As the original experiment did not include simultaneous high-rate current or vibration measurements, it is not possible to confirm the physical origin of the low-frequency class separation.

2.3. Implementation steps

For each trial, the three-phase stator current signals were first processed to remove their mean values. The Clarke transformation was then applied to convert the three-phase currents into the orthogonal (α) and (β) components, and a single current-magnitude signal $M[n]$ was calculated as $\left(M[n] = \sqrt{i_{\alpha}^{2}[n] + i_{\beta}^{2}[n]}\right)$. The resulting signal was centred around the mean and filtered using a second-order Butterworth high-pass filter with a cut-off frequency of 0.2 Hz. Zero-phase forward-backward filtering was then applied to avoid phase distortion. The signal was then normalized by its root mean square (RMS) value. At a sampling frequency of 10 Hz, each trial was divided into 15-second windows containing 150 samples, with a 7.5-second step corresponding to 50% overlap. Twelve windows were retained per trial to maintain a balanced dataset. A 44-dimensional feature vector was extracted from each window. The first group contained 15 general descriptors: mean; standard deviation; RMS; peak magnitude; peak-to-peak value; skewness; kurtosis; crest factor; RMS of the first and second differences; time-domain Shannon entropy; and autocorrelation at lags 1–3. Additionally, the RMS ratio between the 0.2–1 Hz and 1–3 Hz frequency bands was included. Shannon entropy was calculated using 20 histogram bins and a base-2 logarithm. The second group contained 18 ball-oriented descriptors, which were designed to increase sensitivity to weak and irregular ball-fault signatures. These were: impulse factor; clearance factor; zero-crossing count; slope-sign-change count; spectral Shannon entropy; Hjorth activity; mobility and complexity; six TEO statistics (mean; standard deviation; RMS; skewness; kurtosis; and crest factor); and four absolute-envelope descriptors (mean; standard deviation; Shannon entropy; and kurtosis). The TEO was calculated as $\left(\psi[x(n)] = x^{2}(n) - x(n-1)x(n+1)\right)$. Spectral entropy was obtained from the normalized one-sided FFT power spectrum, whereas envelope entropy used 20 histogram bins and a base-2 logarithm.

The final group consisted of autoregressive features. These were estimated using the Yule-Walker method. This method uses model order (p = 10). It provides ten AR coefficients and one prediction-error variance. To emphasize the weak and intermittent characteristics of ball faults, the general, ball-oriented, and AR feature groups were weighted at 1.00, 1.25, and 1.10, respectively before being combined into the final 44-feature vector. During classifier development, standardization and subsequent dimensionality reduction transformations should be estimated only from the training trials within each cross-validation fold, and then

applied unchanged to the held-out trials. The trial-wise separation is of importance due to the overlapping of windows originating from the same physical trial and their statistical dependence. This means that a distribution between the training and testing sets is not possible.

2.4. Algorithms

The classification model $f(x)$ is based on an SVM with an RBF Kernel [30]:

$$f(x) = \sum_{i=1}^{N} \alpha_i y_i K(x_i, x) + b \quad (1)$$

where $K(x_i, x)$ is the Kernel function, α_i is a Lagrange multiplier, y_i is the class label, x_i is a support vector, and b is the bias term. Feature selection uses the Fisher score $F(x_j)$ [31]:

$$F(x_j) = \frac{\sum_{k=1}^{C} n_k (\mu_{k,j} - \mu_j)^2}{\sum_{k=1}^{C} n_k (\sigma_{k,j}^2)} \quad (2)$$

where n_k is the number of training observations in class k, $\mu_{k,j}$ and $\sigma^2_{k,j}$ are the class means and variance of feature j, μ_j is its overall training mean, and C is the number of classes.

Dimensionality reduction is performed using LDA to maximize class separability [32]:

$$W = \frac{|W^T S_B W|}{|W^T S_W W|} \quad (3)$$

where W is the projection matrix, S^B is the between-class scatter matrix, and S^W is the within-class scatter matrix. LDA selects W that maximizes $J(W)$. The overall workflow is summarized in Pseudocode 1.

Pseudocode 1. Proposed bearing fault diagnosis algorithm using fisher score, LDA, and RBF-SVM

INPUT:
- Raw 3-phase current signals S = {Sa, Sb, Sc}
- Labels Y (trial-level), Groups G
- Parameters: winSec = 30, overlap = 50%

OUTPUT:
- Bearing condition:
- Healthy, Ball Fault, or Inner Race Fault

BEGIN

1) PREPROCESSING
   - For each trial:
     - Remove DC offset from three-phase currents
     - Apply Clarke transformation
     - Compute current magnitude
     - Apply 0.2-Hz Butterworth high-pass filter
     - Normalize signal by RMS
2) SEGMENTATION
   - Divide each trial into:
     - 15-s windows (150 samples)
     - 50% overlap (75-sample step)
   - Keep trial identifier G for every window
3) FEATURE EXTRACTION
   - For each window:
     - Extract general statistical features
     - Extract entropy and frequency features
     - Extract ball-oriented, Hjorth, and TEO features
     - Extract AR features (Yule-Walker, order = 10)
     - Combine all descriptors into 44 features
4) GROUPED OUTER VALIDATION
   - Create 7 folds based on trial identifier G
   - For each fold:
   - Hold out:
     - 1 Healthy trial
     - 1 Ball Fault trial
     - 1 Inner Race Fault trial
   - Use remaining 18 trials for training

5) FEATURE PROCESSING
   Using training trials only:
      Standardize features
      Rank features using Fisher Score
      Select top-k features
      Fit LDA
   Apply the same transformations to test trials
6) SVM OPTIMIZATION AND TRAINING
   Using grouped inner validation:
      Tune BoxConstraint (C)
      Tune KernelScale
   Train final RBF-SVM using all outer-training trials
7) WINDOW-LEVEL PREDICTION
   For each test window:
      Predict fault class
      Obtain confidence score
8) TRIAL-LEVEL DECISION
   For each test trial:
      Combine window predictions using
      confidence-weighted voting
      Final class = class with highest weighted score
9) PERFORMANCE EVALUATION
   Repeat for all 7 folds
   Calculate: Accuracy, Precision, Recall, F1-score, Confusion matrix
END

2.5. Validation

Validation was performed using stratified seven-fold cross-validation. The 21 trial identifiers were divided so that each of the seven folds contained three held-out trials: one healthy trial, one ball-fault trial, and one inner-race-fault trial. Consequently, each outer fold was trained using 18 complete trials and tested using three complete trials that had not been seen before. All overlapping windows inherited their parent trial identifier and remained in the same fold. Within each outer training partition, the pre-processing parameters, the Fisher score ranking, the selection of the top k features, the LDA fitting, and the SVM hyperparameter search were fitted using the training data only. The fitted transformations were then applied to the held-out trials. This ordering prevents direct leakage from overlapping windows and avoids the use of test-fold information during model selection.

Robustness and sensitivity boundaries are as follows. The available study did not include an independent motor, an external dataset, a variable-load campaign, a controlled sensor-noise test, or a multirate downsampling experiment. While the grouped procedure addresses leakage between windows, it does not measure domain shift. Consequently, the 100% trial-level point estimate cannot be used as evidence of generalization beyond the tested motor, bearing geometry, sensor chain, operating point, and laboratory environment.

3. RESULTS AND DISCUSSION

Figure 1 shows the full acquisition process: an induction motor drives a DC generator load; a three-phase current sensor feeds a Mega Arduino interface; and a computer performs signal processing. It should be noted that the same motor, load arrangement, sensor chain, and acquisition procedure were used for all three bearing conditions, enabling the comparison to isolate the imposed bearing condition within this controlled setup. The tested motor was rated at 1.5 HP, 220–230 V, 50 Hz, four poles, and approximately 1,400 rpm. The 6203 Z bearing had an inner diameter of 17 mm, an outer diameter of 40 mm, a ball diameter of 6 mm, a pitch diameter of 30 mm, and eight balls.

Figure 2 shows a comparison of representative low-rate current records for healthy, ball-fault, and inner-race-fault conditions. Rather than looking for classical high-frequency fault components, which cannot be resolved at 10 Hz, the reader should look for differences in slow envelope variation and irregularity. Using out-of-fold predictions from seven grouped outer folds, the selected configuration (BoxConstraint = 3, KernelScale = 0.20, LDA without PCA and 12 selected features) correctly classified 70 out of 72 windows (97.22%, Wilson 95% CI: 90.4–99.2%) and all 21 trials (100%, Wilson 95% CI: 84.5–100%).

Table 2 compares three internal configurations that were evaluated using identical grouped folds. The key finding is that the final Fisher-LDA-SVM configuration improved both window- and trial-level performance compared to the two internal alternatives. This is an ablation result, not an external benchmark. Each three-trial test set was classified correctly across the seven outer folds, giving a mean trial accuracy of 100%, an SD of 0 percentage points, a variance of 0, and a range of 0–100%. However, because each fold contained only three independent trials, the zero empirical variability should not be interpreted as indicating robustness at the population level.

Figures 3 and 4 show the aggregated out-of-fold confusion matrices at window and trial levels, respectively. At the window level, all healthy and inner race fault windows were correctly classified, with a recall of 24/24 (100%, Wilson 95% CI: 86.2–100%) for both classes. In contrast, ball fault achieved a recall of 22/24 (91.67%, Wilson 95% CI: 74.2–97.7%), incorrectly classifying two windows as healthy. This error pattern suggests that distinguishing ball fault remains challenging due to its weak and intermittent signatures, which can overlap with normal current variations. Nevertheless, confidence-weighted aggregation corrected these isolated errors at the trial level, where all seven trials in each class were correctly identified. The resulting 100% accuracy at the trial level should be considered alongside the wide Wilson 95% confidence interval (CI) of 64.6–100% per class, reflecting the small number of independent trials rather than definitive evidence of perfect generalization. Figure 5 further illustrates the LDA projection, showing generally compact class clusters with limited boundary overlap. This separation is consistent with the classification results; however, the visualization only represents the current experimental dataset and should not be interpreted as evidence of universal class separability.

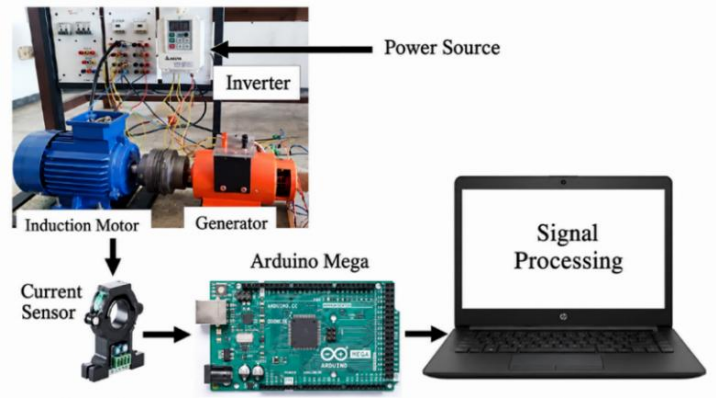

Figure 1. Experimental configuration

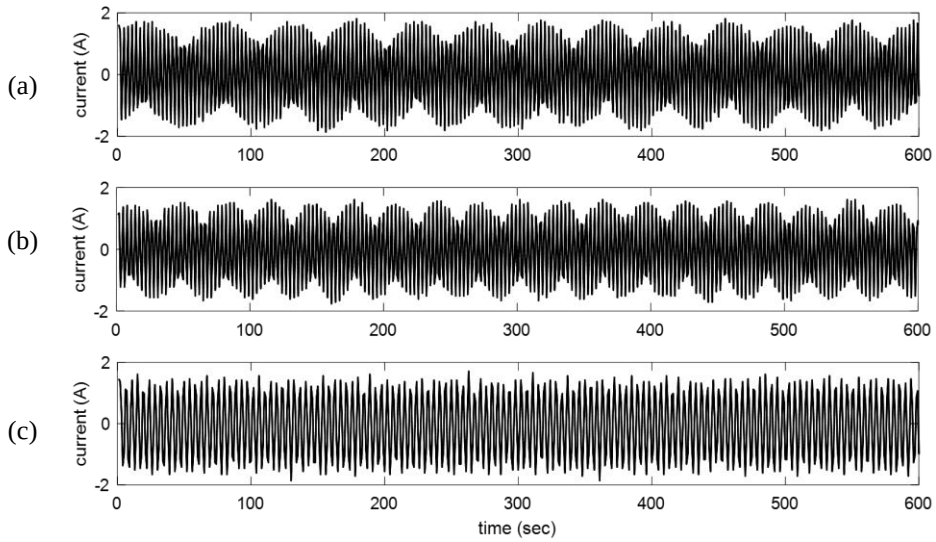

Figure 2. Stator current: (a) normal bearing, (b) bearing with ball defect, and (c) bearing with inner race defect

Table 2. Internal ablation of model configurations using identical grouped folds

Configuration	Key components	recH	recB	recI	AccTrial (%)	AccWindow (%)
Baseline optimized SVM + PCA/LDA	Statistical + entropy + AR + TEO features, feature selection, PCA/LDA, auto-tuned SVM, weighted voting	1.0000	0.8750	1.00	95.83	86.67
Non-optimal tuned setting	Box = 50, KS = 1.50, PCA enabled, maxPC = 12, topFeat = 24	0.8750	0.7500	1.00	87.50	78.30
Final optimized framework	Ball-oriented features + Fisher selection + LDA + optimized SVM + stronger weighted voting	1.0000	1.0000	1.0	100.00	97.22

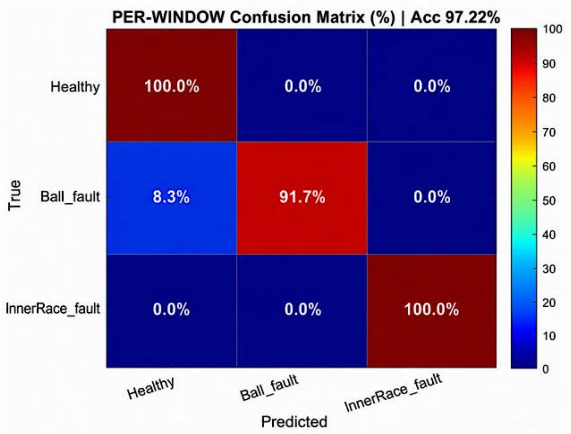

Figure 3. Per-window confusion matrix

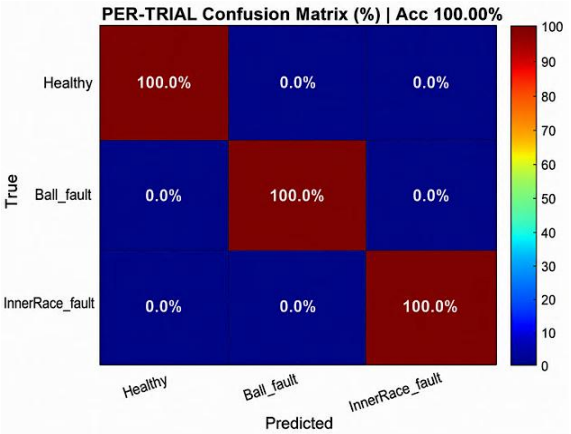

Figure 4. Per-trial confusion matrix

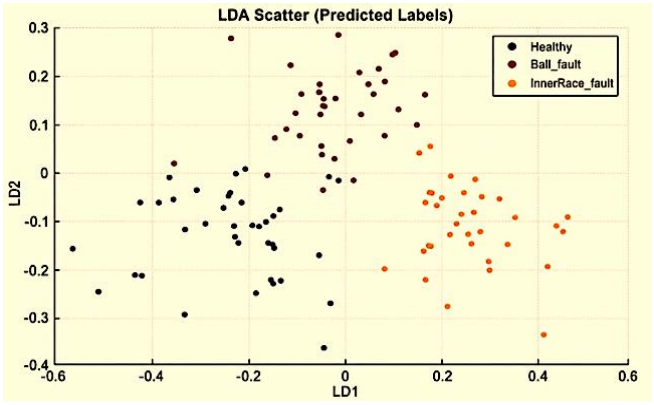

Figure 5. Optimized LDA scatter

Improvements in ball fault recognition are key to understanding the proposed feature-engineering strategy. Ball defects generate weaker and less regular current disturbances than the other evaluated conditions. Consequently, the baseline configuration showed greater overlap between ball fault and healthy samples. The introduction of ball-oriented descriptors, followed by Fisher ranking and the selection of the top 12 features using LDA-based discriminant projection, increased sensitivity to impulsive, irregular, and low-energy signal variations. Internal ablation testing in Table 2 supports this interpretation: the final Fisher-LDA-SVM configuration produced better overall performance than the baseline and non-optimal configurations. However, larger or less appropriate SVM hyperparameters reduced classification performance. These results suggest that for this small data problem, carefully selecting discriminative information was more useful than simply increasing feature dimensionality or classifier complexity. The difference between the results at the window and trial levels also demonstrates the complementary role of decision fusion: feature engineering improves local discrimination, while confidence-weighted voting reduces the influence of a small number of ambiguous windows when forming the final diagnosis. However, this improvement only establishes the value of these components within the present dataset and does not demonstrate superiority over other diagnostic frameworks.

Several controls were implemented to mitigate the optimistic bias associated with the small dataset and overlapping segmentation. Cross-validation was performed by physical acquisition trial rather than by individual window, meaning that all windows originating from a trial were kept exclusively in either the training or test partition. Within each outer fold, normalization, Fisher feature ranking, top-k selection, LDA transformation, and SVM fitting were determined from the outer training trials. Meanwhile, SVM hyperparameters were selected through grouped inner validation, after which the complete pipeline was refitted and evaluated on the untouched outer test trials. This procedure prevents strongly correlated windows from the same experiment from leaking directly into both model development and evaluation. However, grouped validation cannot generate more independent experimental diversity; the study still comprises only 21 physical trials from a single controlled motor-bearing setup. Furthermore, the results do not demonstrate direct observation of classical bearing characteristic frequencies due to the 10-Hz sampling rate having a Nyquist frequency of only 5 Hz. Instead, the discriminative information may arise from lower-frequency electromechanical modulation, envelope variation, or operating-condition-dependent current patterns. Therefore, establishing the physical origin of these features requires synchronized high-rate measurements, followed by controlled downsampling and testing across independent motors and operating regimes.

Consequently, comparisons with previous MCSA, wavelet, vibration-based, and deep-learning studies must be made cautiously. Wavelet and wavelet-scattering approaches can preserve richer time-frequency information; vibration sensors can capture high-frequency mechanical responses directly; and CNN/LSTM-based methods can learn hierarchical representations when large enough datasets and sufficient computational resources are available. In contrast, the present framework investigates whether an engineered-feature representation that is both compact and informative can be achieved through a combination of discriminant learning and SVM classification when sensing bandwidth and independent training data are restricted. As these alternative methods were not reimplemented in the same way across 21 trials with identical partitions, tuning budgets, and evaluation metrics, the present results cannot demonstrate superior accuracy, computational efficiency, or robustness. Furthermore, computational latency, memory consumption, and the cost of embedded implementation were not experimentally benchmarked. The findings should therefore be interpreted as preliminary evidence of feasibility, not as proof of general industrial reliability. Future validation should include larger independent datasets, multiple motors and bearings, variable speeds and loads, different fault severities, controlled noise, external testing or leave-machine-out testing, and direct comparisons with conventional MCSA, vibration, wavelet, and lightweight deep learning methods under identical validation protocols. Such experiments are necessary to determine whether the promising performance observed here can be transferred from controlled laboratory conditions to practical predictive maintenance applications.

4. CONCLUSION

This research evaluated the performance of a bandwidth-aware, physics-informed Fisher-LDA-SVM framework in classifying healthy, ball-fault, and inner-race-fault conditions using 10 Hz three-phase current records. Seven-fold cross-validation produced 70/72 (97.22%; Wilson 95% CI: 90.4–99.2%) correct window predictions and 21/21 (100%; Wilson 95% CI: 84.5–100%) correct trial decisions. Fold-level trial accuracy was 100% in all seven folds; however, each fold contained only three independent test trials. The results support the expectation from feature selection and hybrid learning research that compact, discriminative representations can be useful when data are limited. However, the results neither support nor contradict the reported accuracy of CNN, wavelet, or conventional MCSA studies, as no common experimental benchmark was performed. From a scientific perspective, this work advances the field by separating low-frequency current-trend classification from direct fault-frequency detection. It enforces trial-level grouping throughout model development and reports uncertainty around a point estimate. However, the claims remain limited to one controlled setup. At 10 Hz, the estimated bearing characteristic frequencies are above the Nyquist limit, and external validation is still required in terms of multirate, variable load, fault severity, and noise sensitivity. Therefore, the framework should be regarded as a transparent baseline for the feasibility of future low-cost monitoring studies, rather than as a validated industrial diagnostic system.

ACKNOWLEDGMENTS

The authors would like to express their gratitude to the Ministry of Higher Education, Science, and Technology of the Republic of Indonesia, all individuals, and Universitas Widya Gama Malang, whose support enabled this research to be completed successfully.

FUNDING INFORMATION

This research was fully funded by a DRTPM research grant awarded to PFR Universitas Widya Gama, Malang, Indonesia.

AUTHOR CONTRIBUTIONS STATEMENT

This journal uses the Contributor Roles Taxonomy (CRediT) to recognize individual author contributions, reduce authorship disputes, and facilitate collaboration.

Name of Author	C	M	So	Va	Fo	I	R	D	O	E	Vi	Su	P	Fu
Gigih Priyandoko	✓	✓	✓	✓	✓	✓		✓	✓	✓	✓			
Aviv Yuniar Rahman		✓								✓		✓		

C : **C**onceptualization
M : **M**ethodology
So : **So**ftware
Va : **Va**lidation
Fo : **Fo**rmal analysis
I : **I**nvestigation
R : **R**esources
D : **D**ata Curation
O : Writing - **O**riginal Draft
E : Writing - Review & **E**diting
Vi : **Vi**sualization
Su : **Su**pervision
P : **P**roject administration
Fu : **Fu**nding acquisition

CONFLICT OF INTEREST STATEMENT

The authors confirm that there are no conflicts of interest related to this study.

DATA AVAILABILITY

The data that support the findings of this study are available from the corresponding author, [GP], upon reasonable request.

REFERENCES

[1] B. Brusamarello, J. C. C. Da Silva, K. De M. Sousa, and G. A. Guarneri, "Bearing fault detection in three-phase induction motors using support vector machine and fiber bragg grating," *IEEE Sensors Journal*, vol. 23, no. 5, pp. 4413–4421, 2023, doi: 10.1109/JSEN.2022.3167632.

[2] K. Hamani, M. Kuchar, M. Kubatko, and S. Kirschner, "Advancements in induction motor fault diagnosis and condition monitoring: A comprehensive review," *Sensors*, vol. 25, no. 19, pp. 1–36, 2025, doi: 10.3390/s25195942.

[3] N. El Bouharrouti, D. Morinigo-Sotelo, and A. Belahcen, "Multi-rate vibration signal analysis for bearing fault detection in induction machines using supervised learning classifiers," *Machines*, vol. 12, no. 1, pp. 1–24, 2024, doi: 10.3390/machines12010017.

[4] Z. Wang, D. Shi, Y. Xu, D. Zhen, F. Gu, and A. D. Ball, "Early rolling bearing fault diagnosis in induction motors based on on-rotor sensing vibrations," *Measurement: Journal of the International Measurement Confederation*, vol. 222, pp. 1–15, 2023, doi: 10.1016/j.measurement.2023.113614.

[5] B. H. Bahgat, E. A. Elhay, and M. M. Elkholy, "Advanced fault detection technique of three phase induction motor: comprehensive review," *Discover Electronics*, vol. 1, no. 1, pp. 1–25, 2024, doi: 10.1007/s44291-024-00012-3.

[6] A. Chennana *et al.*, "Vibration signal analysis for rolling bearings faults diagnosis based on deep-shallow features fusion," *Scientific Reports*, vol. 15, no. 1, Mar. 2025, doi: 10.1038/s41598-025-93133-y.

[7] K. F. Brethee, G. R. Ibrahim, and R. A. Mohammed, "Using envelope analysis and compressive sensing method for intelligent fault diagnosis of ball bearing," *Advances in Science, Technology and Engineering Systems*, vol. 5, no. 5, pp. 370–375, 2020, doi: 10.25046/AJ050546.

[8] S. Sun, C. Shen, and D. Wang, "Editorial for special issue: Machine health monitoring and fault diagnosis techniques," *Sensors*, vol. 23, no. 7, pp. 2–5, 2023, doi: 10.3390/s23073493.

[9] N. A. R. Maciejewski, R. Z. Freire, A. L. Szejka, T. P. M. Bazzo, V. B. Frencl, and A. E. Treml, "Comparative analysis of feature selection and classification techniques for robust broken rotor bar diagnosis in induction motors using current and vibration signals," *Autonomous Intelligent Systems*, vol. 5, no. 1, pp. 1–22, 2025, doi: 10.1007/s43684-025-00113-0.

[10] S. Bin Lee *et al.*, "Recent challenges in condition monitoring of industrial electric machines," *IEEE Industrial Electronics Magazine*, vol. 14, no. 4, pp. 158–167, 2020, [Online]. Available: https://hal.archives-ouvertes.fr/hal-03345239

[11] S. Sawai, "Impact of sampling frequency, line parameters, and noise on single-end traveling wave fault location," in *2025 IEEE Kansas Power and Energy Conference, KPEC 2025*, Manhattan, KS, USA: IEEE, 2025, pp. 1–4, doi: 10.1109/KPEC65465.2025.11224758.

[12] E. Baharozu, S. Ilhan, and G. Soykan, "Evaluation of the effects of noise and sampling rate on detection of high impedance fault with machine learning methods on the distribution system," in *Proceedings - 2023 IEEE PES GTD International Conference and Exposition, GTD 2023*, Istanbul, Turkiye: IEEE, 2023, pp. 55–59, doi: 10.1109/GTD49768.2023.00037.

[13] A. Skariah, P. R, R. R, and B. C. R, "Health monitoring of rolling element bearings using improved wavelet cross spectrum technique and support vector machines," *Tribology International*, vol. 154, 2021, doi: 10.1016/j.triboint.2020.106650.

[14] R. N. Toma *et al.*, "Classification framework of the bearing faults of an induction motor using wavelet scattering transform-based features," *Sensors*, vol. 22, no. 22, pp. 1–21, 2022, doi: 10.3390/s22228958.

[15] M. Imane, C. Rahmoune, and D. Benazzouz, "Rolling bearing fault feature selection based on standard deviation and random forest classifier using vibration signals," *Advances in Mechanical Engineering*, vol. 15, no. 4, pp. 1–11, 2023, doi: 10.1177/16878132231168503.

[16] A. Ghediri and N. Goléa, "Induction motor failures detection using motor current signal analysis (MCSA) and two-step support vector machine (SVM) classifier," *Przeglad Elektrotechniczny*, vol. 2024, no. 2, pp. 272–278, 2024, doi: 10.15199/48.2024.02.55.
[17] A. Hassan, A. F. Hashem, A. Sayed, and M. Kayed, "Physics-guided deep learning for acoustic-based fault diagnosis," *International Journal of Engine Research*, vol. 27, no. 3, pp. 337–352, 2026, doi: 10.1177/14680874251361591.
[18] C. Chen, Z. Wang, J. Shi, D. Yue, G. Shi, and C. Wang, "Noise-resilient bearing fault diagnosis via hybrid attention-based multiscale ScConv and quaternion transformer," *IEEE Transactions on Instrumentation and Measurement*, vol. 74, pp. 1–18, 2025, doi: 10.1109/TIM.2025.3593546.
[19] X. Man *et al*., "Wavelet and time domain attention-guided stochastic resonance network for fault diagnosis of rotating machinery in strong noise environment," *Measurement Science and Technology*, vol. 36, no. 7, 2025, doi: 10.1088/1361-6501/adecb6.
[20] A. A. Singh, C. I. Harikrishnan, S. K. Tiwari, and S. Sharma, "Investigation on multi-entropy and multi-statistical features fusion approach for fault detection in rolling bearing using VMD," *IETE Journal of Research*, vol. 69, no. 12, pp. 9245–9250, 2023, doi: 10.1080/03772063.2022.2083707.
[21] D. Yang, Y. Lv, R. Yuan, and Z. Dang, "Fault feature fusion based on entropy-weighted nuisance attribute projection and orthogonal locality preserving projection," in *Sixth International Conference on Electromechanical Control Technology and Transportation (ICECTT 2021)*, Chongqing, China: SPIE, 2022, doi: 10.1117/12.2623849.
[22] H. Zhao, P. Li, A. Guo, and W. Deng, "Lightweight bearing fault diagnosis method based on cross-scale learning transformer under imbalanced data," *Measurement Science and Technology*, vol. 35, no. 10, 2024, doi: 10.1088/1361-6501/ad5ea4.
[23] Z. Wang, H. Lu, Y. Shi, and X. Wang, "Lightweight CNN architecture design based on spatial–temporal tensor and its application in bearing fault diagnosis," *IEEE Transactions on Instrumentation and Measurement*, vol. 73, pp. 1–12, 2024, doi: 10.1109/TIM.2023.3336435.
[24] L. Jiang, C. Shi, H. Sheng, X. Li, and T. Yang, "Lightweight CNN architecture design for rolling bearing fault diagnosis," *Measurement Science and Technology*, vol. 35, no. 12, 2024, doi: 10.1088/1361-6501/ad7a1a.
[25] Z. Tong, W. Li, B. Zhang, H. Gao, X. Zhu, and E. Zio, "Bearing fault diagnosis based on discriminant analysis using multi-view learning," *Mathematics*, vol. 10, no. 20, 2022, doi: 10.3390/math10203889.
[26] Z. Zhang, S. Xu, and H. Chen, "Discriminative feature learning and selection with label-induced sparse filtering for intelligent fault diagnosis of rotating machinery," *Mechanical Systems and Signal Processing*, vol. 196, 2023, doi: 10.1016/j.ymssp.2023.110338.
[27] Y. Li, X. Gu, and Y. Wei, "A deep learning-based method for bearing fault diagnosis with few-shot learning," *Sensors*, vol. 24, no. 23, 2024, doi: 10.3390/s24237516.
[28] X. Liang, M. Zhang, G. Feng, D. Wang, Y. Xu, and F. Gu, "Few-shot learning approaches for fault diagnosis using vibration data: A comprehensive review," *Sustainability*, vol. 15, no. 20, 2023, doi: 10.3390/su152014975.
[29] D. A. Moysidis, G. D. Karatzinis, Y. S. Boutalis, and Y. L. Karnavas, "A study of noise effect in electrical machines bearing fault detection and diagnosis considering different representative feature models," *Machines*, vol. 11, no. 11, 2023, doi: 10.3390/machines11111029.
[30] A. P. Gopi, R. N. S. Jyothi, V. L. Narayana, and K. S. Sandeep, "Classification of tweets data based on polarity using improved RBF kernel of SVM," *International Journal of Information Technology (Singapore)*, vol. 15, no. 2, pp. 965–980, 2023, doi: 10.1007/s41870-019-00409-4.
[31] R. Kumar and R. S. Anand, "Bearing fault diagnosis using multiple feature selection algorithms with SVM," *Progress in Artificial Intelligence*, vol. 13, no. 2, pp. 119–133, 2024, doi: 10.1007/s13748-024-00324-1.
[32] W. Jia, M. Sun, J. Lian, and S. Hou, "Feature dimensionality reduction: a review," *Complex and Intelligent Systems*, vol. 8, no. 3, pp. 2663–2693, 2022, doi: 10.1007/s40747-021-00637-x.

BIOGRAPHIES OF AUTHORS



Gigih Priyandoko received his Bachelor of Engineering (B.Eng.) degree in electrical engineering from Universitas Brawijaya, Malang, Indonesia, in 1991; his Master of Engineering (M.Eng.) degree in electrical engineering from Institut Teknologi Bandung, Indonesia, in 1996; and his Doctor of Philosophy (Ph.D.) degree in mechanical engineering from Universiti Teknologi Malaysia, Malaysia, in 2009. He is currently a faculty member at Universitas Widya Gama, Malang, Indonesia, where he is actively involved in teaching and research in electrical engineering and intelligent systems. His research interests include the application of artificial intelligence in electrical engineering, particularly intelligent control systems, signal processing, and AI-based optimization for power systems and mechatronic systems. He can be contacted at email: gigih@widyagama.ac.id.



Aviv Yuniar Rahman received his Bachelor of Engineering (B.Eng.) degree in electrical engineering, specializing in computer engineering and telematics, in 2013, and his Master of Engineering (M.Eng.) degree in electrical engineering, with a specialization in intelligent multimedia networks, in 2017, both from Institut Teknologi Sepuluh Nopember, Surabaya, Indonesia. He subsequently received his Doctor of Philosophy (Ph.D.) degree in information and communication technology from Asia e University, Subang Jaya, Malaysia, in 2026. Since 2014, he has been a lecturer in the Department of Informatics Engineering at Universitas Widya Gama, Malang, Indonesia. His research interests include image processing, computer vision, deep learning, and natural language processing, particularly the development of intelligent computational models for complex data interpretation. He can be contacted at email: aviv@widyagama.ac.id.